BB

ISSN 1346-244X
RIKEN-AF-NP-387

N/Z dependence of Core Polarization Charges and Quadrupole Moments of B-isotopes

H. Sagawa and K. Asahi

March 2001

The Institute of Physical and Chemical Research (RIKEN)
2-1 Hirosawa, Wako, Saitama 351-0198, Japan
TEL: (048)462-1111 FAX: (048)462-4642
e-mail: *username*@rikvax.riken.go.jp

N/Z dependence of Core Polarization Charges and Quadrupole Moments of B-isotopes

H. Sagawa[1] and K. Asahi[2],[3]

[1] *Center for Mathematical Sciences, University of Aizu,*

Ikki-machi, Aizu-Wakamatsu, Fukushima 965-8580, Japan

[2]*Department of Physics,*

Tokyo Institute of Technology, Oh-okayama 2-12-1, Meguro-ku, Tokyo 152-8551, Japan

[3] *The Institute of Physical and Chemical Research (RIKEN), 2-1 Hirosawa, Wako, Saitama 351-0198, Japan*

Phys. Rev. **C** (June, 2001) in press.

Abstract

N/Z dependence of core polarization charges for electric quadrupole transitions is studied in C-isotopes by using a microscopic particle-vibration model in which Hartree-Fock and random phase approximations are used to calculate the single-particle wave functions and giant quadrupole resonances. A large quenching of the polarization charges is found in nuclei with large N/Z ratio. Recent experimental data of quadrupole moments of ^{15}B and ^{17}B are reproduced well by using the calculated polarization charges for shell model wave functions.

PACS numbers : 21.10.Pc,21.10.Re,21.60.Jz,23.20.Js

I. INTRODUCTION

Recently, precise measurements of electric quadrupole moments (Q-moments) become possible in nuclei far from stability line by the use of radioactive nuclear beams [1-3]. These data make it possible to study N/Z dependence of the effective charges up to the ratio N/Z ~2.5. In nuclei far from stability, it is expected that the core polarization is weakly induced by particles with extended tail due to small binding energies and small orbital angular momentum (ℓ =0 or 1) [4,5]. This is because those particles spend an appreciable amount of time outside of the core of nucleus and, thus, cannot efficiently polarize the core. This decoupling effect between the core and valence particles is expected to occur in the polarization charges and also in low energy electric dipole transitions in nuclei near drip lines [6]. In the present work, we study a quenching feature of core polarization charges in relation with the quadrupole moments of B-isotopes near the stability line to the neutron drip line.

The present study of core polarization is performed by using a microscopic model which combines the particle-vibration coupling model, and the self-consistent Hartree-Fock (HF) and the random phase approximation (RPA) theory with the use of a Skyrme interaction [7,4,5]. At the first stage, we calculate the single-particle wave functions and giant resonances (GR) by using the self-consistent HF and RPA theory. In RPA calculations, we take into account the coupling to the continuum solving the Green's function in the coordinate space [8,9]. Then, the core polarization is evaluated by using the particle-vibration coupling model [10] with RPA collective states and HF single particle wave functions [7]. We use the SIII interaction as an effective interaction for our numerical calculations of core polarizations. It is shown in the literature [4] that the the interaction dependence is very small for the core polarization charges. We check the interaction dependence with another Skyrme interaction SkM*. Since the present model of the particle-vibration coupling is described somewhere in detail [5], we give a brief description of our model in

Section 2. RPA and core polarization results are discussed in Section 3. In Section 4, the quadrupole moments (Q-moments) of B-isotopes are studied by using shell model wave functions together with the obtained core polarization charges and HF single-particle wave functions. Conclusions are given in Sections 5.

II. MICROSCOPIC PARTICLE-VIBRATION COUPLING MODEL

We perform first the HF calculation and, then, solve the RPA Green's function using a Skyrme interaction SIII, consistently. The neutron and proton degree of freedom is taken into account explicitly in the RPA calculations. This freedom is particularly important to study GR and core polarizations in nuclei near the neutron drip lines. The RPA Green's function G_{RPA} is expressed as

$$\begin{aligned} G_{RPA} &= G^{(0)} + G^{(0)} v_{ph} G_{RPA} \\ &= (1 - G^{(0)} v_{ph})^{-1} G^{(0)} \end{aligned} \tag{1}$$

with the unperturbed Green's function $G^{(0)}$ and the particle-hole interaction v_{ph} [11]. The RPA response function is solved in the coordinate space including the effect of the coupling to the continuum. The RPA strength function is then obtained by

$$S(E) \equiv \sum_n |< n \mid Q^\lambda \mid 0 >|^2 \, \delta(E - E_n) = \frac{1}{\pi} Im\, Tr(Q^{\lambda\dagger} G_{RPA}(E)\, Q^\lambda) \tag{2}$$

where Q^λ expresses one-body operators

$$Q_\mu^{\lambda=2,\,\tau=0} = \sum_{i=1}^{A} r_i^2 Y_{2\mu}(\hat{r}_i) \qquad \text{for isoscalar quadrupole modes,} \tag{3}$$

$$Q_\mu^{\lambda=2,\tau=1} = \sum_{i=1}^{A} \tau_z r_i^2 Y_{2\mu}(\hat{r}_i) \qquad \text{for isovector quadrupole modes,} \tag{4}$$

and

$$Q_\mu^{\lambda=2,el} = e\sum_{i=1}^{Z} r_i^2 Y_{2\mu}(\hat{r}_i) = \frac{e}{2}\sum_{i=1}^{A}(1-\tau_z) r_i^2 Y_{2\mu}(\hat{r}_i) \qquad \text{for electric quadrupole modes.} \quad (5)$$

The unperturbed strength can be obtained replacing $G_{RPA}(E)$ by the unperturbed response function $G_0(E)$ in Eq. (1).

In order to estimate the polarization due to the core excitations, we use a perturbation with RPA phonons [10,7,5]. The perturbed single-particle wave function is expressed as

$$|\,\tilde{i}\,> = |\,i\,> + \sum_{j,\omega_\lambda} \frac{<(j\times\omega_\lambda)i\mid V_{pv}\mid i>}{\varepsilon_i - (\varepsilon_j+\omega_\lambda)}\mid (j\times\omega_\lambda)i> . \quad (6)$$

where V_{pv} is the particle-vibration coupling interaction. The reduced transition matrix element for the one-body operator Q^λ is modified as

$$<\tilde{j}\|Q^\lambda\|\tilde{i}> = <j\|Q^\lambda\|i> + \sum_{\omega_\lambda} \frac{2\omega_\lambda}{(\varepsilon_i-\varepsilon_j)^2-\omega_\lambda^2} \frac{\sqrt{2i+1}<(j\times\omega_\lambda)i\mid V_{pv}\mid i>}{\sqrt{2\lambda+1}} <\omega_\lambda\|Q^\lambda\|0> . \quad (7)$$

The particle-vibration coupling V_{pv} is derived from the Skyrme interaction approximating the momentum derivative operators $\mathbf{k}$ and $\mathbf{k}'$ by the Fermi momentum $\mathbf{k_F}$ so that one can use directly the RPA transition densities for the calculation of the matrix element. This approximation was made only for the construction of the particle-vibration coupling Hamiltonian. Then, the isoscalar (IS) and the isovector (IV) coupling interactions are expressed as

$$V_{pv}(\vec{r_1}-\vec{r_2}) = \begin{cases} V_{pv}^{\tau=0}(r)\delta(\vec{r_1}-\vec{r_2}) & \text{for} \quad \tau=0 \\ V_{pv}^{\tau=1}(r)\delta(\vec{r_1}-\vec{r_2})\tau_{z1}\cdot\tau_{z2} & \text{for} \quad \tau=1 \end{cases} \quad (8)$$

where

$$V_{pv}^{\tau=0}(r) = \{\frac{3}{4}t_0 + \frac{3}{48}(\alpha+2)(\alpha+1)t_3\rho^\alpha(r) + \frac{1}{8}k_F^2[3t_1+t_2(5+4x_2)]\}, \quad (9)$$

$$V_{pv}^{\tau=1}(r) = \{-\frac{1}{4}t_0(1+2x_0) - \frac{1}{24}t_3(1+2x_3)\rho^\alpha(r) + \frac{1}{8}k_F^2[-t_1(1+2x_1)+t_2(1+2x_2)]\}, \quad (10)$$

and $r = \frac{1}{2}(r_1+r_2)$. Then the coupling matrix is evaluated to be

$$< (j \times \omega_\lambda)i \mid V_{pv}^{\tau} \mid i > = \frac{1}{\sqrt{2i+1}} \int r^2 dr V_{pv}^{\tau}(r) \delta\rho(r) R_j(r) R_i(r) < j \| Y_\lambda \| i > \qquad (11)$$

where $\delta\rho(r)$ is the radial transition density defined by

$$\delta\rho(\vec{r}) \equiv \delta\rho(r)\, Y_{\lambda\,\mu}(\hat{r}) \qquad (12)$$

and $R(r)$ expresses the radial wave functions of single-particle states. In Eqs. (9) and (10), the contributions from the momentum-dependent forces, t_1- and t_2-terms, can be effectively included by renormalizing the value of t_0 . The renormalization factor in the case of SIII interaction is 0.83 for the IS interaction and 0.81 for the IV interaction. Thus, the effect of the momentum-dependent forces on the coupling interaction is slightly less than 20% for both the IS and IV channels.

In the present calculations, we estimate the polarization charges using a method in which the particle-vibration coupling V_{pv} includes both the IS and the IV part,

$$V_{pv}(r)\,\delta\rho(r) = V_{pv}^{\tau=0}(r)\,[\,\delta\rho_{IS}^{n}(r) + \delta\rho_{IS}^{p}(r)\,] + \tau_z^{particle}\, V_{pv}^{\tau=1}(r)\,[\,\delta\rho_{IV}^{n}(r) - \delta\rho_{IV}^{p}(r)\,] \qquad (13)$$

where $[\,\delta\rho_{IS}^{n}(r) + \delta\rho_{IS}^{p}(r)\,]$ and $[\,\delta\rho_{IV}^{n}(r) - \delta\rho_{IV}^{p}(r)\,]$ are the radial transition densities of the responses to the external IS and the IV fields in (3) and (4), respectively. In the present continuum calculation the transition density at a given energy is very likely a superposition of contributions from many states with different dynamical structure. Thus, the neutron (proton) part of the IS transition density $\delta\rho_{IS}^{n}$ ($\delta\rho_{IS}^{p}$) at a given energy may not necessarily be the same as that of the IV transition density $\delta\rho_{IV}^{n}$ ($\delta\rho_{IV}^{p}$) at the same energy, in contrast to the case of an isolated quantum state. In the latter case the neutron (or proton) part of the quadrupole transition density is uniquely defined, irrespective of the response to the external IS or IV field, namely ; $\delta\rho_{IS}^{n} = \delta\rho_{IV}^{n}$ and $\delta\rho_{IS}^{p} = \delta\rho_{IV}^{p}$. In the present model, the proton transition density $\delta\rho^{p}$ for the calculation of $< \omega_\lambda \| Q^{\lambda=2,\,el} \| 0 >$ is obtained from the response to the external electric field (5). The

transition density $\delta\rho^p$ is again not necessarily the same as either $\delta\rho^p_{IS}$ or $\delta\rho^p_{IV}$ which are used in the calculations of Eq. (13). The electric polarization charges for quadrupole moments are defined as

$$e_{pol} = \frac{<\tilde{j}\| Q^{\lambda=2,el} \|\tilde{i}>}{<j\| Q^{\lambda=2,\tau=0} \|i>} - (\frac{1}{2} - t_z)e \quad . \tag{14}$$

The IS (IV) polarization charge e^{IS}_{pol} (e^{IV}_{pol}) is obtained from the first (second) term contribution containing $V^{\tau=0}_{pv}$ ($V^{\tau=1}_{pv}$) in the particle-vibration coupling (13). Then, the total electric polarization charge is written as

$$e_{pol} = \begin{cases} e^n_{pol} = e^{IS}_{pol} + e^{IV}_{pol} & \text{for neutrons} \\ \\ e^p_{pol} = e^{IS}_{pol} - e^{IV}_{pol} & \text{for protons} \end{cases} \tag{15}$$

In Eq. (15),$e^{IS}_{pol}(e^{IV}_{pol})$ for neutrons is in general different from $e^{IS}_{pol}(e^{IV}_{pol})$ for protons. The electric effective charge is defined as $e^n_{eff} = e^n_{pol}$ for neutrons and $e^p_{eff} = e^p_{pol} + e$ for protons.

III. GQR AND CORE POLARIZATIONS

We have performed HF+RPA calculations for ^{12}C, ^{16}C and ^{20}C using a Skyrme SIII interaction. The HF ground state in ^{12}C is obtained by the filling approximation from the bottom of the potential up to $1p_{3/2}$ proton and neutron states in the HF potential. In ^{20}C, the neutron orbitals are occupied up to the $1d_{5/2}$ state, while the $1d_{5/2}$ state is partially occupied in ^{16}C.

The IS, IV and electric quadrupole responses in ^{12}C to the fields (3), (4) and (5) are shown in Fig. 1 (a) together with the unperturbed response to the field (3) (the unperturbed response to the field (4) is the same as that to the field (3) by definition). The IS giant quadrupole resonance (GQR) peak is found at Ex=22.7MeV. This GQR peak is a typical IS state, having 50%−50% mixing of the proton and neutron amplitudes

with the same signs. The strength in the energy region 15 $\leq$Ex$\leq$ 28MeV exhausts 70% of the IS energy weighted sum rule (EWSR) value. The first 2^+ state is found in the RPA response at Ex=6.08MeV having B(IS,λ=2)=86.4fm^4 which correspond to 9% of the EWSR value. Main configurations of the first 2^+ state are IS-type coherent proton and neutron ($1p_{3/2} \rightarrow 1p_{1/2}$) excitations. Since shell model calculations in Section 4 will be performed by taking into account the full p-shell configurations, it will be a double-counting if we include the first 2^+ state for the core polarization calculations. Therefore, we will discard the effect of the first 2^+ state for the following core polarization calculations in all C-isotopes. The IV strength is distributed in a wide energy region 20 $\leq$Ex$\leq$ 50 MeV. The summed strength in this energy region exhausts 72% of the IV EWSR value.

The quadrupole responses in ^{16}C and ^{20}C to the fields (3), (4) and (5) are shown in Figs. 1 (b) and 1 (c), respectively. We found low energy 2^+ states due to $0\hbar\omega$-type excitations at around 6MeV also in both ^{16}C and ^{20}C. The main configurations are a proton ($1p_{3/2} \rightarrow 1p_{1/2}$) excitation and neutron sd-shell configurations. We discard these low-energy states below 10MeV in the following core polaization calculations since the $0\hbar\omega$ configurations are fully taken into account in the shell model study. We can see a large neutron threshould effect in the response even in the IS GQR energy region in the two isotopes. The IS GQR peak is found at Ex=22.8MeV (21.3MeV) in ^{16}C (^{20}C) with a larger width than that of ^{12}C. The summed strength in the energy region 15MeV $\leq$Ex$\leq$ 28MeV exhausts 76% (69%) of the IS EWSR value in ^{16}C (^{20}C). Since the low energy strength below Ex=15MeV is governed by neutron excitations to the continuum in the two nuclei, the IS and IV responses have almost the same strength in this energy region. In ^{16}C, there is substantial IV strength below the IS GQR peak. The IV strength below the IS GQR peak is even larger in ^{20}C due to the large mass asymmetry effect [5]. The main IV strength is found above Ex=28MeV in ^{16}C. The summed strength 28 $\leq$Ex$\leq$ 50MeV exhausts 58% of the IV EWSR. Two main IV peaks are found in ^{20}C at

around Ex=32 and 40MeV. The summed strength 28 $\leq$Ex$\leq$ 50MeV exhausts 47% of the IV EWSR. In all three nuclei, only very small IS strength is found in the energy regoin above Ex=30MeV. This feature confirms that the IV peaks are rather good IV states having equal amounts of proton and neutron amplitudes with opposite signs.

The calculated static polarization charges for ^{12}C core with SIII interaction are listed in Table I (a), in which the single-particle energy difference is set to be $\varepsilon_i - \varepsilon_j$=0 in Eq. (7). The results with SkM* are shown in Table I (b). Since $1d_{3/2}$ proton and neutron states are unbound, the configurations involving $1d_{3/2}$ orbits are not calculated in Table I. Averaged polarization charges for p-shell orbits with SIII (SkM*) force are $e_{pol}(n)$=0.53e (0.52e) and $e_{pol}(p)$=0.29e (0.29e), which are equivalent to the empirical effective charges $e_{eff}(n)$=0.5e and $e_{eff}(p)$=1.3e commonly used in light nuclei [14,12]. The calculated polarization charges for sd-shell configrations are smaller than those of p-shell configurations and very much state dependent. The transition densities of IS and IV GQR at various energies are shown in Fig. 2 (a), while the single particle wave functions are drawn in Fig. 2 (b). As is seen in Figs. 2 (a) and (b), the $1p_{3/2}$ wave function and the IS GQR transition density at Ex=22.7MeV have the peaks close to the rms mass radius r_{rms}=2.3fm so that the overlap is large in Eq.(11). For IV GQR, the transition densities are energy dependent. The $\delta\rho$ for the peak at the highest energy Ex=38.5MeV has the same surface peak as the IS one. The peak of $\delta\rho$ at Ex=32.6MeV is shifted to inside of the surface , while the $\delta\rho$ at Ex=27.9MeV has a node at 2fm largely affected by ($1p_{3/2} \rightarrow 2p_{3/2}$) excitations. Thus, the two IV densities at Ex=27.9 and 32.6MeV have less overlap than those at Ex=22.7 and 38.5MeV and give smaller contributions to the polarization charges. Since the single-particle wave functions for the sd-shell orbits are extended largely for outside, the overlaps with the transition densities of GQR become worse than those of the p-shell wave functions. As is expected from Eq. (11), a smaller overlap gives a smaller core polarization effect , as is the case for sd-shell configurations.

Especially the $2s_{1/2}$ state has a node at r=2.5fm and a largely extended tail, which make much smaller overlaps with the transition densities than the other orbits, and give a large quenching for the polarization charges. To check the interaction dependence, the results with SkM* are given in Table I (b). We can see in Tables I (a) and (b) that the two results are very close each other within few % differences for all configurations except that with the loosely-bound $2s_{1/2}$ state.

In Tables II and III (a) , the static IS and IV polarization charges calculated with SIII interaction are tabulated for ^{16}C and ^{20}C, respectively. The polarization charges for ^{20}C are also given in Table III (b) with SkM* interaction. We can see in Tables III (a) and III (b) that the interation dependence is again very small both in the cases of p-shell configurations and sd-shell configurations. The IS and IV quadrupole transition densities at various energies in ^{20}C are shown in Fig. 3 (a). A clear difference is seen between the transition densities at Ex= 12.5MeV near the threshould and at Ex=21.3MeV near the IS GQR. The former has two radial nodes and a very extended tail, while the latter shows a typical Tassie type radial dependence as a collective surface mode peaked at the nuclear surface r = 2.9fm. The unique shape of radial transition density of the low-energy threshold strength leads to the destructive contribution to the polarization charge. The two IV densities at Ex=32.5 and 39.7MeV have peaks at somewhat inside of the surface. The HF neutron single-particle wave functions in ^{20}C are shown in Fig. 3 (b). The peak of the $1d_{5/2}$ wave function is close to the surface so that $e_{pol}(IS)$ with $1d_{5/2}$-orbit is large and becomes almost the same values as those of p-shell configurations. The $2s_{1/2}$ neutron orbit is a loosely-bound orbit with the separation energy S=2.0MeV and $1d_{3/2}$ neutron orbit is a resonance state at ε_{res}=3.3MeV. These two orbits have very extended wave functions and the configurations with the two orbits give much smaller $e_{pol}(IS)$ values than that of $1d_{5/2}$-orbit, because of small integrals in Eq. (11) and also large expectation values for $Q^{\lambda,\tau=0}$ in the denominator of the first term of Eq. (14). On the other hand, all

sd-shell proton orbits are well bound in ^{20}C and have almost the same values of $e_{pol}(IS)$ as those for the p-shell configurations.

In the RPA results in ^{16}C and ^{20}C, the proton amplitudes are quenched below the IS GQR peaks. The summed B(E2) value in the energy region 15MeV $\leq$Ex$\leq$ 28MeV is 56.6, 40.5 and 31.3 e^2fm^4 for A=12, 16 and 20, respectively. Thus the proton transition amplitude $< \omega_\lambda \| Q^{\lambda=2,el} \| 0 >$ in Eq. (7) is smaller for heavier isotopes and gives smaller IS part of the polarization charge. The calculated $e_{pol}(IS)$ value decreases rapidly as a function of N/Z to be 0.41, 0.29 and 0.15 for the neutron p-shell configurations in ^{12}C, ^{16}C and ^{20}C, respectively. On the other hand, the proton strength below IV GQR remains to be almost the same magnitude in all three isotopes. Thus, the $e_{pol}(IV)$ value is rather constant to be $0.12e$ ($0.12e$), $0.14e$ ($0.15e$) and 0.13 e ($0.14e$) for the neutron (proton) p-shell configurations in ^{12}C, ^{16}C and ^{20}C, respectively.

In general, the IS mode is expected to give rise to the IV moment proportional to the neutron excess $(N-Z)/A$ because of the preservation of local ratio of protons to neutrons [10]. This assumption holds approximately in the RPA results in which large IV components are found below the IS GQR peaks in Figs. 1 (b) and 1 (c). Then, the IS contributions to the core polarization charges is expected to have $e(1-\frac{N-Z}{A})/2 = eZ/A$ dependence because of the cancellation between the IS and IV moments in the electric moment obtained from (5). On the other hand, the RPA results in Figs. 1 (b) and 1 (c) show that the IV GQR peaks have very small IS components. Then, a ratio of electric to the IV quadrupole moment from Eq. (5) is expected to be $-e/2$. This ratio suggests the IV polarization to be independent of the N/Z ratio, while the IS ones might decrease largely due to the excess neutrons. The N/Z dependence of polarization charges in Tables I, II and III are qualitatively understood by the nature of IS and IV GQR.

The N and Z dependence of the polarization charges is given in Eq. $(6-386b)$ in ref. [10] as

$$e_{pol} = e\,(\frac{Z}{A} - 0.32\,\frac{N-Z}{A} + (0.32 - 0.3\,\frac{N-Z}{A})\,\tau_z). \qquad (16)$$

This formula is derived by using the single collective GQR state both for the IS and IV mode exhausting 100% of the EWSR. The effect of the coupling of IV mode to IS mode is included in the first and the fourth terms of the formula. Namely, the N/Z dependence of the first term is due to the effect of IV moment in the IS mode and the fourth term takes into account the change of the coupling potential due to the coupling between the IS and IV mode. The second and the third terms are obtained by the assumption of no changes in the total density for the IV mode, which is equivalent to no induced IS moment in the IV mode. If we apply literally Eq. (16) to the present C-isotopes, we obtain

$$e_{pol} = e\,(0.50 + 0.32\,\tau_z) \qquad for \qquad {}^{12}_{6}\mathrm{C}_6 \qquad (17)$$

and

$$e_{pol} = e\,(0.30 + 0.25\,\tau_z) \qquad for \qquad {}^{16}_{6}\mathrm{C}_{10} \qquad (18)$$

and

$$e_{pol} = e\,(0.17 + 0.20\,\tau_z) \qquad for \qquad {}^{20}_{6}\mathrm{C}_{14} \qquad (19)$$

The e^{IS}_{pol} part of ${}^{12}_{6}\mathrm{C}_6$ in (17) is 20% larger than the values for p-shell configurations in Table I (a), while the values for ${}^{16}_{6}\mathrm{C}_{10}$ and ${}^{20}_{6}\mathrm{C}_{14}$ are very close to the present p-shell results in Tables II and III (a). The smaller e^{IS}_{pol} values for the p-shell orbits of ${}^{12}_{6}\mathrm{C}_6$ in Table I are due to dispersion of the IS strength in the high energy region above Ex=28MeV. The agreement between the two results in ${}^{16}_{6}\mathrm{C}_{10}$ and ${}^{20}_{6}\mathrm{C}_{14}$ might be rather accidental since the different results in ${}^{12}_{6}\mathrm{C}_6$ are compensated by the different properties of IS GQR in the two heavier isotopes. The property of the IS GQR in the two neutron-rich nuclei is considerably influenced by the large neutron excess together with the presence of the threshold strength in the present RPA results, which gives weaker N/Z dependence of the

$e_{pol}^{IS}(n)$. On the other hand, no continuum effect is considered in the formula (16). The IV part of the polarization charges in Eqs. (17), (18) and (19) are very different from the present results. The formula (16) has N/Z dependence also for the IV part, which turns out to be differences of more than a factor 2 in ${}^{12}_{6}C_6$ and 40~50% in ${}^{16}_{6}C_{10}$ and ${}^{20}_{6}C_{14}$ compared with the values e_{pol}(IV) in Tables I, II and III. This difference is due to the stronger IV coupling in ref. [10] than the present one of Eq. (10).

The N/Z dependence of the proton and neutron polarization charges are shown in Fig. 4. The average neutron polarization charges for p-shell configurations decrease as a function of the neutron numbers; $e_{pol}(n)$=0.53e, 0.44e and 0.28e for ^{12}C, ^{16}C and ^{20}C, respectively. The polarization charges for protons have stronger N/Z dependence as $e_{pol}(p)$=0.29e, 0.16e and 0.03e for ^{12}C, ^{16}C and ^{20}C, respectively. This is because of a bigger quenching effect in the IS part than the IV part. The N/Z dependence of the $e_{pol}(n)$ of sd-shell orbits is rather weak because of the loosely-bound nature of these orbits in ^{12}C. On the other hand, the proton $e_{pol}(p)$ values of the sd-shell configurations decrease rapidly from ^{16}C to ^{20}C since they are well-bound. The formula (16) gives also a strong N/Z dependence of e_{pol} ; $e_{pol}(n)$=0.82e, 0.56e and 0.37e, and $e_{pol}(p)$=0.18e, 0.04e and -0.05e for ^{12}C, ^{16}C and ^{20}C, respectively. The main reason of the difference between the two models is due to the difference in the e_{pol}^{IV} values.

IV. Q-MOMENT OF B-ISOTOPES

We apply now the obtained polarization charges to the calculations of Q-moments in B-isotopes. The shell model wave functions are obtained by using the program OXBASH [13] with the effective interaction WBT by Warburton and Brown [15]. We take into account the model space with full p-shell and full sd-shell configurations without $2\hbar\omega$-type configurations mixing between p-shell and sd-shell. Namely, the model space of B-isotopes with $A \leq 13$ is $(1p)^{A-4}$-configurations, while $(1p)^9(2s1d)^{A-13}$-configurations

are adopted for the isotopes with $A > 13$. We perform also the shell model calculations with another interaction PSDMK2 by Millener and Kurath [14] and obtain almost the identical results for Q-moments of B-isotopes. The Q-moment for the shell model wave function with spin I can be expressed as a linear combination of the single-particle matrix elements

$$< IM = I|Q^{\lambda=2,el}_{\mu=0}|IM = I > = \frac{1}{\sqrt{2I+1}} < II20|II >< I||Q^{\lambda=2,el}||I >$$
$$= \frac{1}{\sqrt{2I+1}} < II20|II > \sum_{i,j} C_{I,I}(i,j) < j||Q^{\lambda=2,el}||i > \quad (20)$$

where $C_{I,I}(i,j)$ is the structure factor (one-body transition density) of the shell model state I and $|i(j) >$ is the HF single particle state. The single-particle matrix element $< j||Q^{\lambda=2,el}||i >$ in Eq. (20) is replaced by the modified one (7) to take into account the core polarization effect.

The calculated results are given in Table IV and Fig. 5 with experimental data [17,18,1,3]. The results in Table IV are obtained by using the calculated polarization charges for two different shell model wave functions of the WBT and PSDMK2 interactions. The results with the constant effective charges are given in Fig. 5 for the shell model wave functions of the WBT interaction. As a reference system, we choose an appropriate C-isotope which has close N/Z ratio to that of each B-isotope, to select the polarization charges and HF wave functions. Namely, the core polarization charges and the HF wave functions of ^{12}C are applied to calculate the Q-moments of ^{10}B, ^{11}B and ^{12}B. The corresponding values of ^{16}C are used for ^{13}B and ^{14}B, while those of ^{20}C are used for ^{15}B and ^{17}B. The calculations are also performed by using harmonic oscillator wave functions with the oscillator length b =1.67fm and the empirical effective charges e^p_{eff}=1.3 and e^n_{eff}=0.5.

From ^{10}B to ^{13}B, the two calculations in Fig. 5 give essentially the same results and show excellent agreement with the experimental data. An important issue drawn by this

agreement is that the present particle-vibration model reveals the microscopic origin of the effective charges in stable light nuclei and gives a quantitative justification of the adopted values in the standard shell model calculations. The two results in Fig. 5 deviates slightly in ^{13}B and ^{14}B, and the conventional method with the constant effective charges gives few % larger Q-moments than the present model. The difference between the two calculations becomes larger in ^{15}B and ^{17}B as much as 40%. It is clearly seen in Fig. 5 that the present results show excellent agreement with the experimental data, but the conventional model does not. This agreement justifies a conjecture of the large quenching of the polarization charges in nuclei near drip lines. The two different effective interactions for the shell model calculations are used for the results in Table IV. While both the two results give fine agreement with the experimental data, the results of PSDMK2 is somewhat larger than those of WBT interaction , especially in the odd-odd isotopes. Further quantitative check of our prediction might be done in the Q-moments and B(E2) values of other drip line nuclei. For example, our model predicts the Q-moment of ^{17}C with $I = 3/2$ to be 17.2mb with the WBT interaction, while the conventional model gives 30.8mb. Since the Q-moment of ^{17}C is dominated by the neutron configurations, it might be interesting to measure experimentally this moment in order to clarify the quenching of the neutron polarization charges.

V. CONCLUSIONS

In conclusion, using a particle-vibration coupling together with the HF wave functions and the RPA response functions in ^{12}C, ^{16}C and ^{20}C, we have studied the N/Z dependence of the quadrupole polarization charges. We found that both the neutron and proton polarization charges decrease rapidly as a function of N/Z ratio. It is shown also that the state dependence of the polarization charges are large especially in ^{16}C and ^{20}C even in a given major shell. We applied the obtained polarization charges to calculate the Q-moments of

B-isotopes. We found that the present microscopic model gives excellent agreement with the experimental data of all B-isotopes from ^{10}B to ^{17}B, while the conventional model fails to reproduce the experimental Q-moments of ^{15}B and ^{17}B. From the results obtained in the present paper we can make a conclusion that the N/Z dependence is crucial to reproduce the experimental Q-moments of drip line nuclei and a fixed polarization charge in the shell model calculations is questionable to use even in a given major shell.

We would like to thank I. Hamamoto for enlightening discussions. We are also grateful to H. Ogawa for useful discussions from the experimental side. This work is supported in part by the Japanese Ministry of Education, Science, Sports and Culture by Grant-In-Aid for Scientific Research under the program number C(2) 12640284.

REFERENCES

[1] H. Izumi, K. Asahi, H. Ueno. H. Okuno, H. Sato, K. Nagata, Y. Hori, M. Adachi, N. Aoi, A. Yoshida, G. Liu , N. Fukunishi and M. Ishihara, Phys. Lett. **B366**, 51 (1996).

[2] H. Ogawa, K. Asahi, K. Sakai, A. Yoshimi, M. Tsuda, Y. Uchiyama, T. Suzuki, K. Suzuki, N.Kurokawa, M. Adachi, H. Izumi, H. Ueno, T. Shimoda, S. Tanimoto, N. Takahashi, W.-D.Schmidt-Ott, M. Schaefer, S. Fukuda, A. Yoshida, M. Notani, T. Kubo, H. Okuno, H. Sato, N. Aoi, K. Yoneda, H. Iwasaki, N. Fukuda, N. Fukunishi, M. Ishihara, and H. Miyatake, Phys. Lett. **B451**, 11 (1999).

[3] H. Ogawa, K. Sakai, H. Ueno, T. Suzuki, H. Miyoshi, K. Asahi, M. Nagakura, K. Yogo, A. Goto, T. Suga, T. Honda, N. Imai, Y.X. Watanabe, K. Yoneda, N. Fukuda, H. Yoshimi, N. Aoi, Y. Kobayashi, W.-D. Schmidt-Ott, G. Neyens, A. Yoshida, T. Kubo, and M. Ishihara, Proc. of RIKEN Symposium on "Shell Model 2000" (Wako-shi, Japan, March 2000) to appear in Nucl. Phys. A (2001).

[4] I.Hamamoto and H.Sagawa, Phys. Rev. **C54**, 2369 (1996).

[5] I.Hamamoto, H.Sagawa and X.Z.Zhang, Nucl. Phys. **A626**, 669 (1997).

[6] H. Sagawa, Toshio Suzuki, H. Iwasaki and M. Ishihara, Phys. Rev. **C** (February, 2001) in press.

[7] H. Sagawa and B. A. Brown, Nucl. Phys. **A430**, 84 (1984).

[8] S. Shlomo and G. F. Bertsch, Nucl. Phys. **A243**, 507 (1975).

[9] Nguyen Van Giai and H. Sagawa, Nucl. Phys. **A371**, 1 (1981).

[10] A.Bohr and B.R.Mottelson, Nuclear Structure, Vol.II, W.A.Benjamin, Reading, Massachusetts (1975).

[11] I.Hamamoto, H.Sagawa and X.Z.Zhang, Phys. Rev. **C55**, 2361 (1997).

[12] B.A.Brown, R.Radhi and B.H.Wildenthal, Phys. Reports **101**, 313 (1983).

[13] OXBASH, The Oxford, Buenos-Aires, Michigan State, Shell Model Program, B. A. Brown, A. Etchegoyen and W. D. M. Rae, MSU Cyclotron Laboratory Report No. 524 (1986).

[14] D. J. Millener and D. Kurath, Nucl. Phys. **A255**,315 (1975).

[15] E. K. Warburton and B. A. Brown, Phys. Rev. **C46**, 923 (1992) and private communications.

[16] S. Cohen and D. Kurath, Nucl. Phys. **73**, 1 (1965).

[17] P. Raghavan, Atomic Data and Nuclear Data Tables **42**, 189 (1989).

[18] T. Minamisono, T. Ohtsubo, I. Minami, S. Fukuda, A. Kitagawa, M. Fukuda, K. Matsuta, Y. Nojiri, S. Takeda, H. Sagawa and H. Kitagawa, Phys. Rev. Lett. **69**, 2058 (1992).

TABLES

TABLE I. Static IS and IV core polarization charges calculated for neutron and proton orbitals in ^{12}C: (a) with SIII force and (b) with SkM* force. The e_{pol}(IS) and e_{pol}(IV) values are obtained by using Eqs. (7) and (14) with $\varepsilon_i - \varepsilon_j$=0. The $B(\lambda=2)_{sp}$ value for the transition from the state $|i>$ to $|f>$ is calculated with the charges $e_n = e_p$=1 for each configuration using the HF wave functions. The values for the proton $2s_{1/2}$ configuration are not given in the table since this orbit is unbound in the HF potential. See the text for details.

(a) SIII		neutrons			protons		
f	i	$B(\lambda=2)_{sp}(fm^4)$	e_{pol}(IS)	e_{pol}(IV)	$B(\lambda=2)_{sp}(fm^4)$	e_{pol}(IS)	e_{pol}(IV)
$1p_{3/2}$	$1p_{3/2}$	3.57	0.423	0.122	3.69	0.418	0.121
$1p_{1/2}$	$1p_{3/2}$	4.17	0.398	0.115	4.35	0.390	0.113
$1d_{5/2}$	$1d_{5/2}$	11.84	0.282	0.081	14.60	0.246	0.071
$2s_{1/2}$	$1d_{5/2}$	15.00	0.132	0.040			

(b) SkM*		neutrons			protons		
f	i	$B(\lambda=2)_{sp}(fm^4)$	e_{pol}(IS)	e_{pol}(IV)	$B(\lambda=2)_{sp}(fm^4)$	e_{pol}(IS)	e_{pol}(IV)
$1p_{3/2}$	$1p_{3/2}$	3.71	0.421	0.115	3.84	0.416	0.114
$1p_{1/2}$	$1p_{3/2}$	4.52	0.390	0.107	4.73	0.383	0.105
$1d_{5/2}$	$1d_{5/2}$	11.32	0.294	0.081	13.23	0.266	0.074
$2s_{1/2}$	$1d_{5/2}$	12.77	0.172	0.049			

TABLE II. Static IS and IV core polarization charges calculated for neutron and proton orbitals in ^{16}C with SIII force. The neutron $1d_{3/2}$ state is a resonance state in HF potential at e_{res}=3.8MeV. The real part of the $1d_{3/2}$ wave function is obtained to adjust the box radius of HF calculation in the coordinate space to fit the unbound single-particle energy at the resonance energy. See the text and the captions to Table I for details.

		neutrons			protons		
f	i	$B(\lambda=2)_{sp}(fm^4)$	e_{pol}(IS)	e_{pol}(IV)	$B(\lambda=2)_{sp}(fm^4)$	e_{pol}(IS)	e_{pol}(IV)
$1p_{3/2}$	$1p_{3/2}$	4.32	0.299	0.147	4.00	0.315	0.154
$1p_{1/2}$	$1p_{3/2}$	4.75	0.287	0.141	4.29	0.309	0.150
$1d_{5/2}$	$1d_{5/2}$	13.10	0.227	0.104	9.24	0.287	0.130
$2s_{1/2}$	$1d_{5/2}$	15.20	0.133	0.059	7.83	0.230	0.099
$1d_{3/2}$	$1d_{5/2}$	4.79	0.145	0.068	2.89	0.241	0.110
$1d_{3/2}$	$1d_{3/2}$	47.32	0.070	0.035	18.39	0.171	0.079
$2s_{1/2}$	$1d_{3/2}$	41.35	0.067	0.032	15.27	0.161	0.072

TABLE III. Static IS and IV core polarization charges calculated for neutron and proton orbitals in ^{20}C: (a) with SIII force and (b) with SkM* force. The neutron $1d_{3/2}$ state is a resonance state in SIII (SkM*) HF potential at e_{res}=3.3 (2.1) MeV. See the text and the captions to Tables I and II for details.

(a) SIII		neutrons			protons		
f	i	$B(\lambda=2)_{sp}(fm^4)$	e_{pol}(IS)	e_{pol}(IV)	$B(\lambda=2)_{sp}(fm^4)$	e_{pol}(IS)	e_{pol}(IV)
$1p_{3/2}$	$1p_{3/2}$	4.49	0.153	0.132	4.33	0.166	0.141
$1p_{1/2}$	$1p_{3/2}$	4.68	0.149	0.128	4.47	0.165	0.139
$1d_{5/2}$	$1d_{5/2}$	13.37	0.140	0.108	9.04	0.178	0.138
$2s_{1/2}$	$1d_{5/2}$	14.13	0.108	0.078	6.64	0.178	0.127
$1d_{3/2}$	$1d_{5/2}$	4.80	0.087	0.067	2.56	0.168	0.129
$1d_{3/2}$	$1d_{3/2}$	85.59	0.031	0.023	10.97	0.154	0.118
$2s_{1/2}$	$1d_{3/2}$	47.08	0.047	0.034	9.00	0.157	0.112

(b) SkM*		neutrons			protons		
f	i	$B(\lambda=2)_{sp}(fm^4)$	e_{pol}(IS)	e_{pol}(IV)	$B(\lambda=2)_{sp}(fm^4)$	e_{pol}(IS)	e_{pol}(IV)
$1p_{3/2}$	$1p_{3/2}$	4.79	0.169	0.144	4.43	0.177	0.152
$1p_{1/2}$	$1p_{3/2}$	5.26	0.165	0.138	4.76	0.177	0.150
$1d_{5/2}$	$1d_{5/2}$	13.89	0.149	0.107	9.76	0.178	0.132
$2s_{1/2}$	$1d_{5/2}$	13.64	0.124	0.078	7.51	0.172	0.110
$1d_{3/2}$	$1d_{5/2}$	4.91	0.103	0.071	2.86	0.168	0.120
$1d_{3/2}$	$1d_{3/2}$	63.59	0.048	0.031	13.11	0.152	0.105
$2s_{1/2}$	$1d_{3/2}$	33.45	0.070	0.043	10.7	0.152	0.096

TABLE IV. Q-moments of B-isotopes. Calculated values are obtained by using the shell model wave functions and the core polarization charges in Table I (a) for A=10,11 and 12, those in Table II for A=13 and 14 and those in Table III (a) for A = 15 and 17. The WBT and PSDMK2 interactions are used for the shell model calculations, while the core polarization charges are obtained by using SIII interaction. Experimental data are taken from ref. [17] for $A = 10, 11$ and 13 , ref. [18] for A = 12, ref. [1] for A=14 and 15, and ref. [3] for A=17. The experimental value for A=13 in ref. [17] is re-evaluated by taking the new value of Q_{exp} for A=12 in the table as a reference. For details, see the text.

A	J^π	Q_{cal}(mb)(WBT)	Q_{cal}(mb)(PSDMK2)	Q_{exp}(mb)
10	3^+	82.1	90.6	84.72 ± .56
11	$\frac{3}{2}^-$	40.6	45.2	40.65 ± .26
12	1^+	11.3	19.0	13.21 ± 0.26
13	$\frac{3}{2}^-$	36.3	36.5	36.9 ± 1.0
14	2^-	18.4	27.6	29.84 ± .75
15	$\frac{3}{2}^-$	37.2	39.1	38.01 ± 1.08
17	$\frac{3}{2}^-$	39.2	40.7	38.8 ± 1.5

FIGURES

FIG. 1. The unperturbed and the RPA strength functions for the IS, the IV and the charge quadrupole mode in $^{12}_{6}C_6$ (a), $^{16}_{6}C_{10}$ (b) and $^{20}_{6}C_{14}$ (c) as a function of excitation energy. The operators (3), (4) and (5) are used for the calculations of the IS, the IV and the charge quadrupole response, respectively. The unperturbed strength function is the same for the IS and the IV operators. The SIII interaction is used.

FIG. 2. (a) The radial transition densities of the RPA IS and IV quadrupole excitations in $^{12}_{6}C_6$ at various excitation energies, Ex , as a function of radial coordinate. The IS density is obtained at Ex=22.7MeV, while the IV densities are obtained at Ex=27.9, 32.6 and 38.5MeV. The dotted line at r=2.3fm shows the HF mass rms radius of $^{12}_{6}C_6$. The SIII interaction is used.
(b) The HF wave functions in $^{12}_{6}C_6$ calculated by SIII interaction. The dotted line at r=2.3fm shows the HF rms mass radius of $^{12}_{6}C_6$. See the text for details.

FIG. 3. (a) The radial transition densities of the RPA IS and IV quadrupole excitations in $^{20}_{6}C_{14}$ at various excitation energies, Ex, as a functions of radial coordinate. The IS densities are obtained at Ex=12.5 and 21.3MeV, while the IV densities are obtained at Ex=32.5 and 39.7MeV. The dotted line at r=2.9fm shows the HF mass rms radius of $^{20}_{6}C_{14}$. The SIII interaction is used.
(b) The HF wave functions in $^{20}_{6}C_{14}$ calculated by SIII interaction. The dotted line at r=2.9fm shows the HF rms radius of $^{20}_{6}C_{14}$. See the text for details.

FIG. 4. Calculated static core polarization charges in ^{12}C, ^{16}C and ^{20}C as a function of N/Z ratio; (a) for neutrons and (b)for protons. The e_{pol}(n) and e_{pol}(p) values are obtained by using Eq. (15) with the results in Tables I (a), II and III (a). The SIII interaction is used. Each configuration is classified by a different symbol; circles for ($1p_{3/2}$, $1p_{3/2}$), squares for ($1p_{1/2}$, $1p_{3/2}$), diamonds for ($1d_{5/2}$, $1d_{5/2}$), up-triangles for ($2s_{1/2}$, $1d_{5/2}$), plus signs for ($1d_{3/2}$, $1d_{5/2}$), down-triangles for ($1d_{3/2}$, $1d_{3/2}$) and stars for ($2s_{1/2}$, $1d_{3/2}$) configurations, respectively. The p-shell configurations are connected by solid lines, while the sd-shell configurations are connected by dashed lines. See the text and the captions to Tables I, II and III for details.

FIG. 5. Calculated and experimental Q-moments of B-isotopes. The solid line is the results with the polarization charges in Tables I (a), II and III (a) and HF single-particle wave functions , while the dashed line is obtained by using the constant effective charges e^p_{eff}=1.3 and e^n_{eff}=0.5 and the harmonic oscillator wave functions with the oscillator length b=1.67fm. The effective interaction WBT is used for the shell model calculations. Experimental data are taken from refs. [17,18,1,3]. See the text and the captions to Table IV for details.

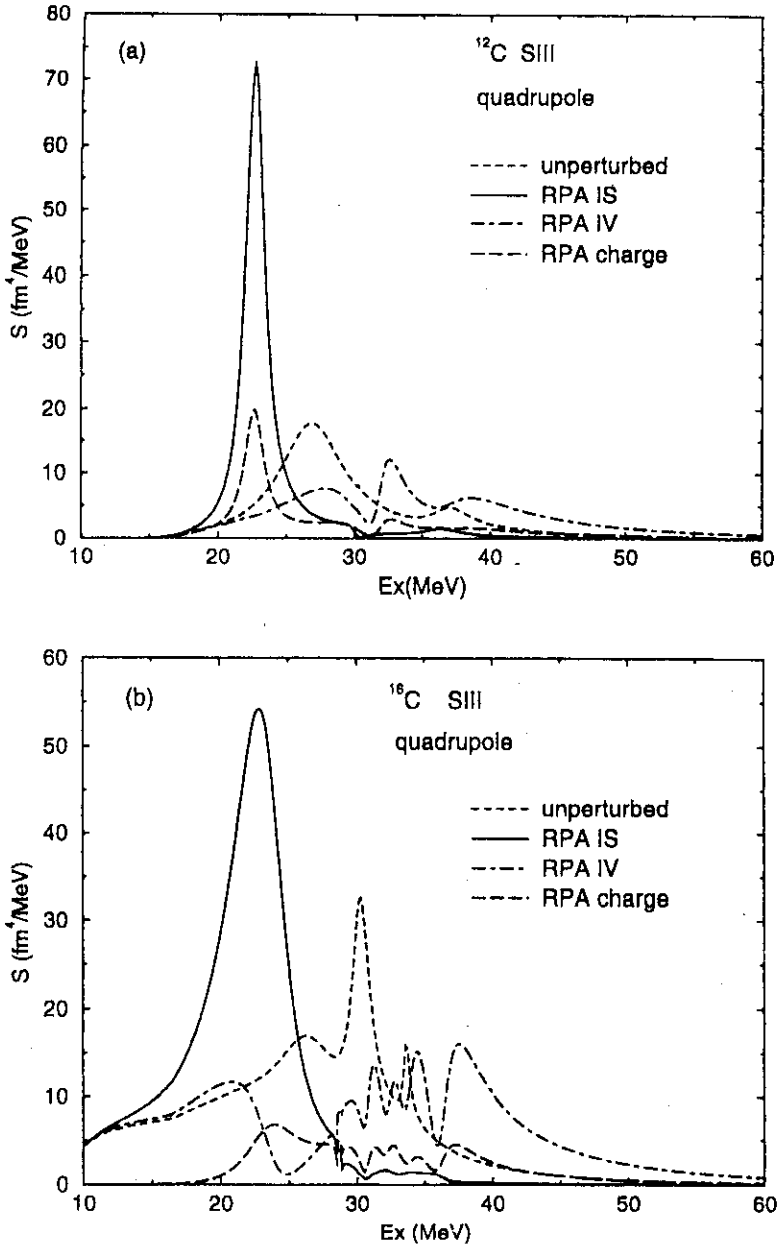
(a)
^{12}C SIII
quadrupole
unperturbed
RPA IS
RPA IV
RPA charge
S (fm^4/MeV)
Ex(MeV)
(b)
^{16}C SIII
quadrupole
unperturbed
RPA IS
RPA IV
RPA charge
S (fm^4/MeV)
Ex (MeV)
(c)
^{20}C SIII
quadrupole
unperturbed
RPA IS
RPA IV
RPA charge
S(fm^4/MeV)
Ex (MeV)

FIG. 1.

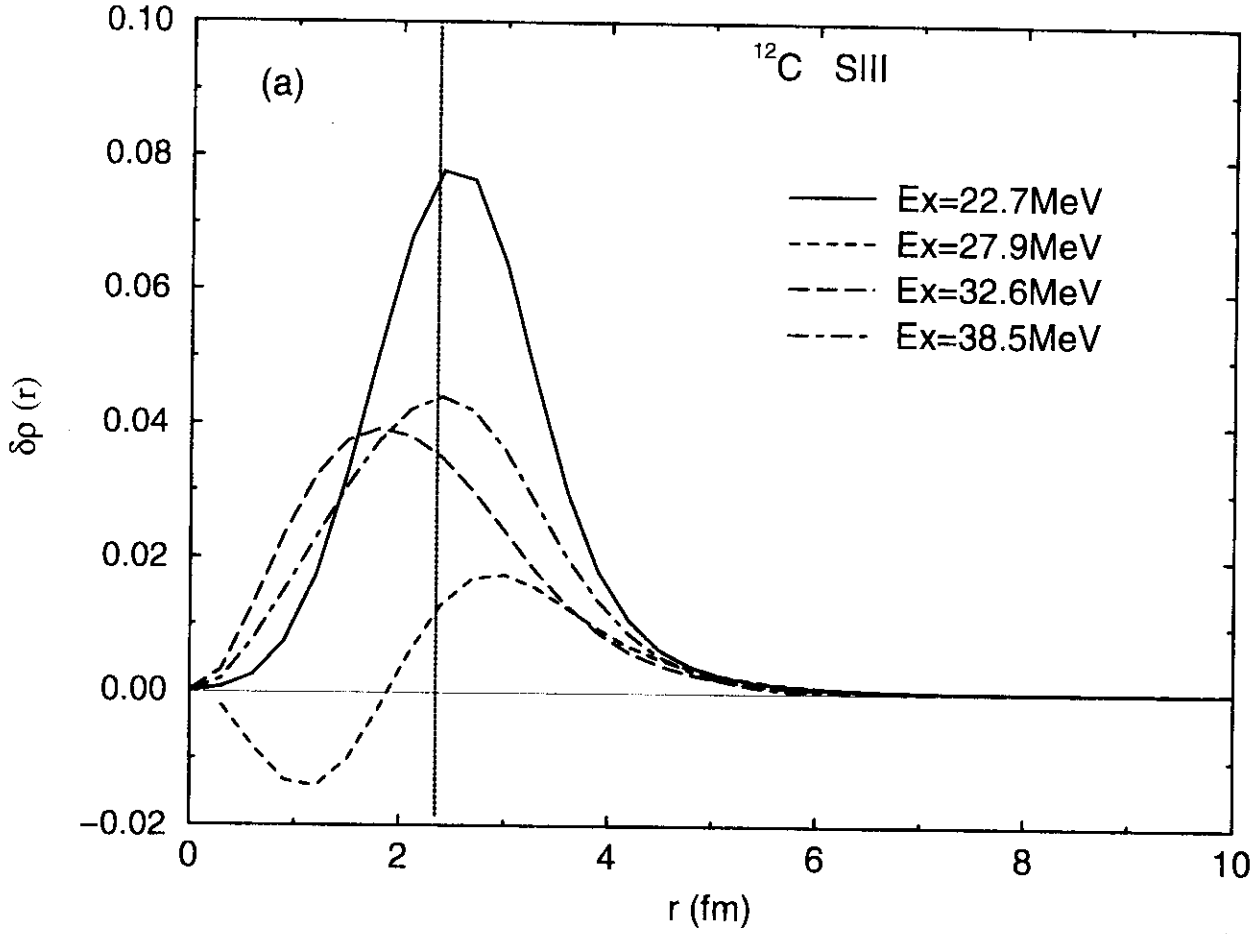
(a)
^{12}C SIII
Ex=22.7MeV
Ex=27.9MeV
Ex=32.6MeV
Ex=38.5MeV
δρ (r)
r (fm)
0.10
0.08
0.06
0.04
0.02
0.00
−0.02
0
2
4
6
8
10

FIG. 2.

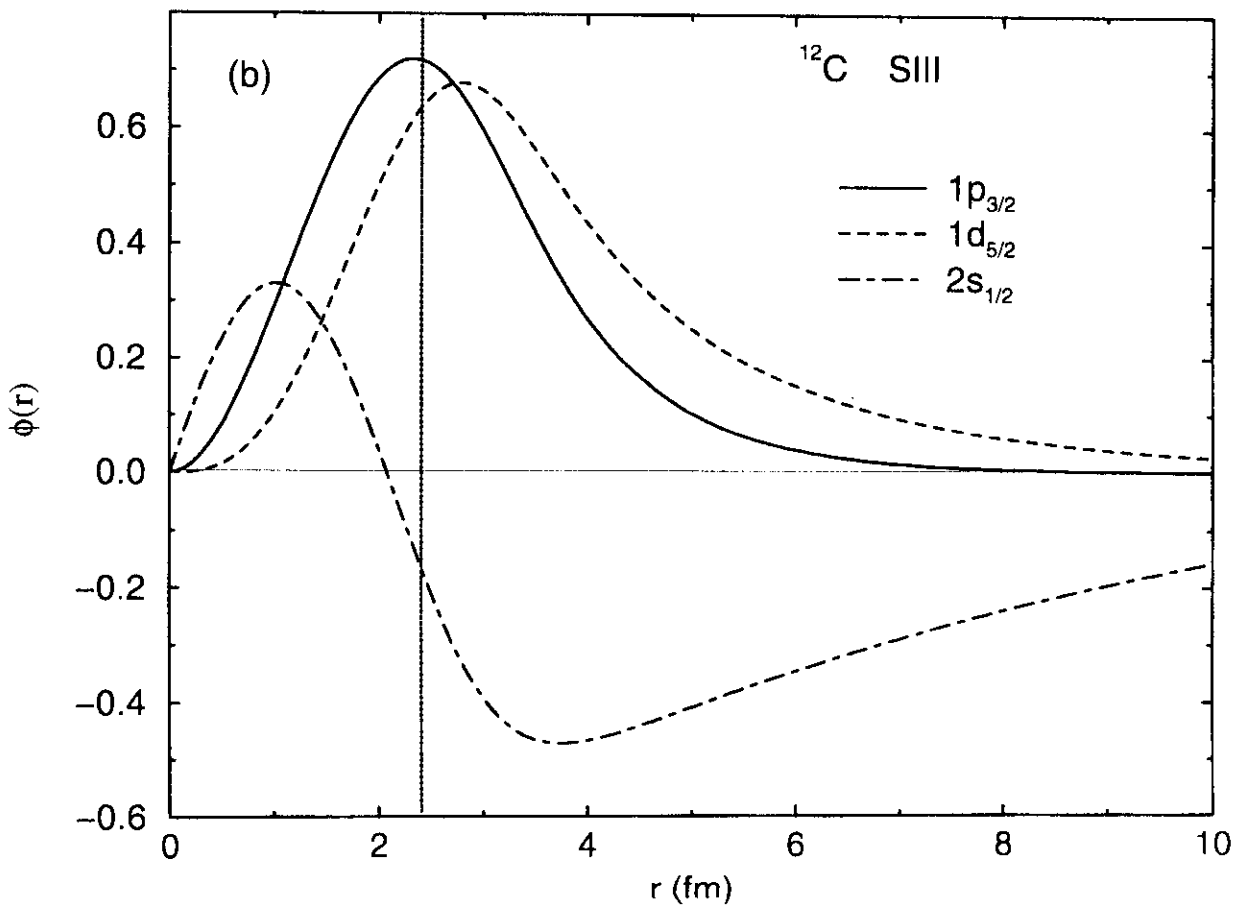
(b)
^{12}C SIII
$1p_{3/2}$
$1d_{5/2}$
$2s_{1/2}$
φ(r)
r (fm)
0.6
0.4
0.2
0.0
−0.2
−0.4
−0.6
0
2
4
6
8
10

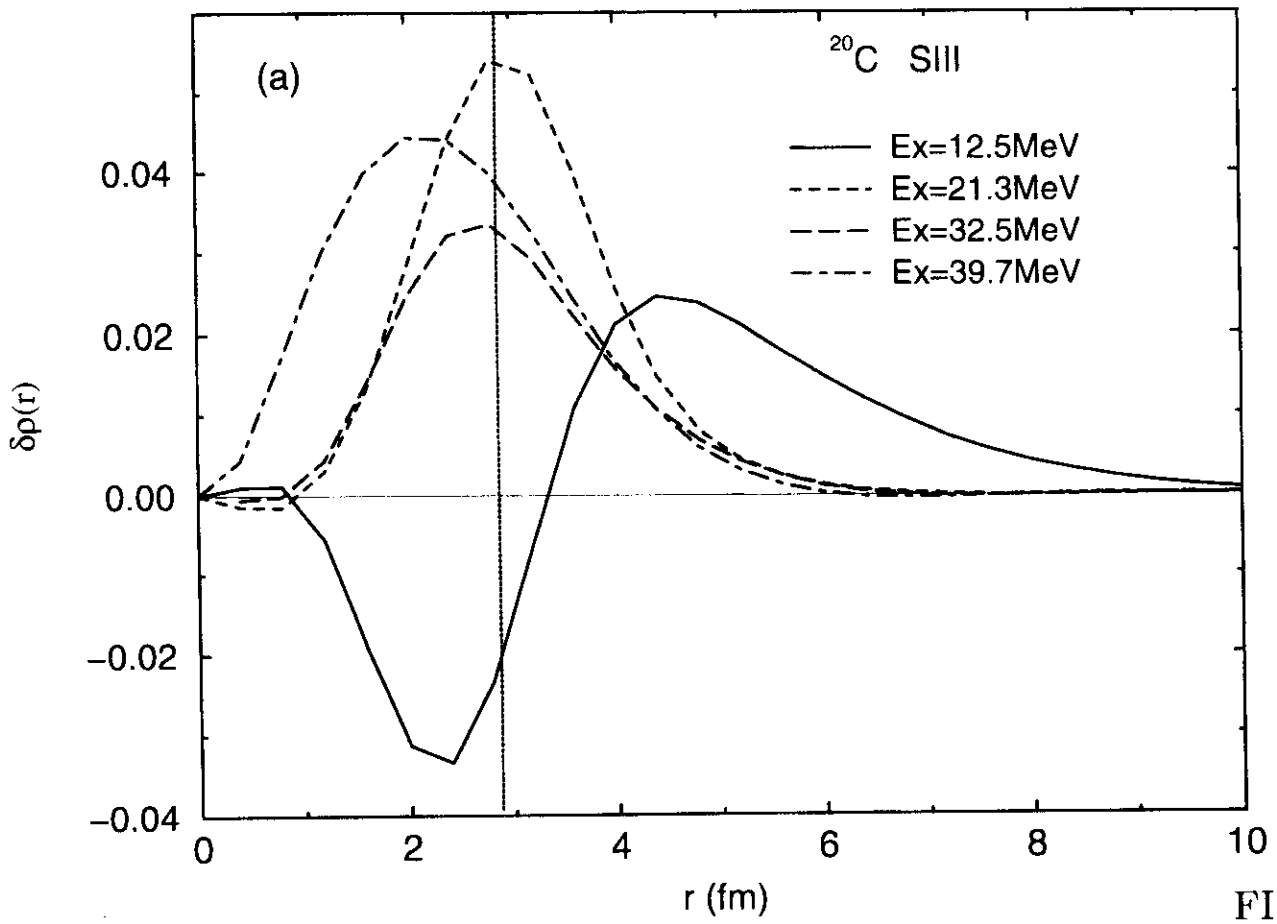
(a)
^{20}C SIII
Ex=12.5MeV
Ex=21.3MeV
Ex=32.5MeV
Ex=39.7MeV
δρ(r)
0.04
0.02
0.00
−0.02
−0.04
0
2
4
6
8
10
r (fm)

FIG. 3.

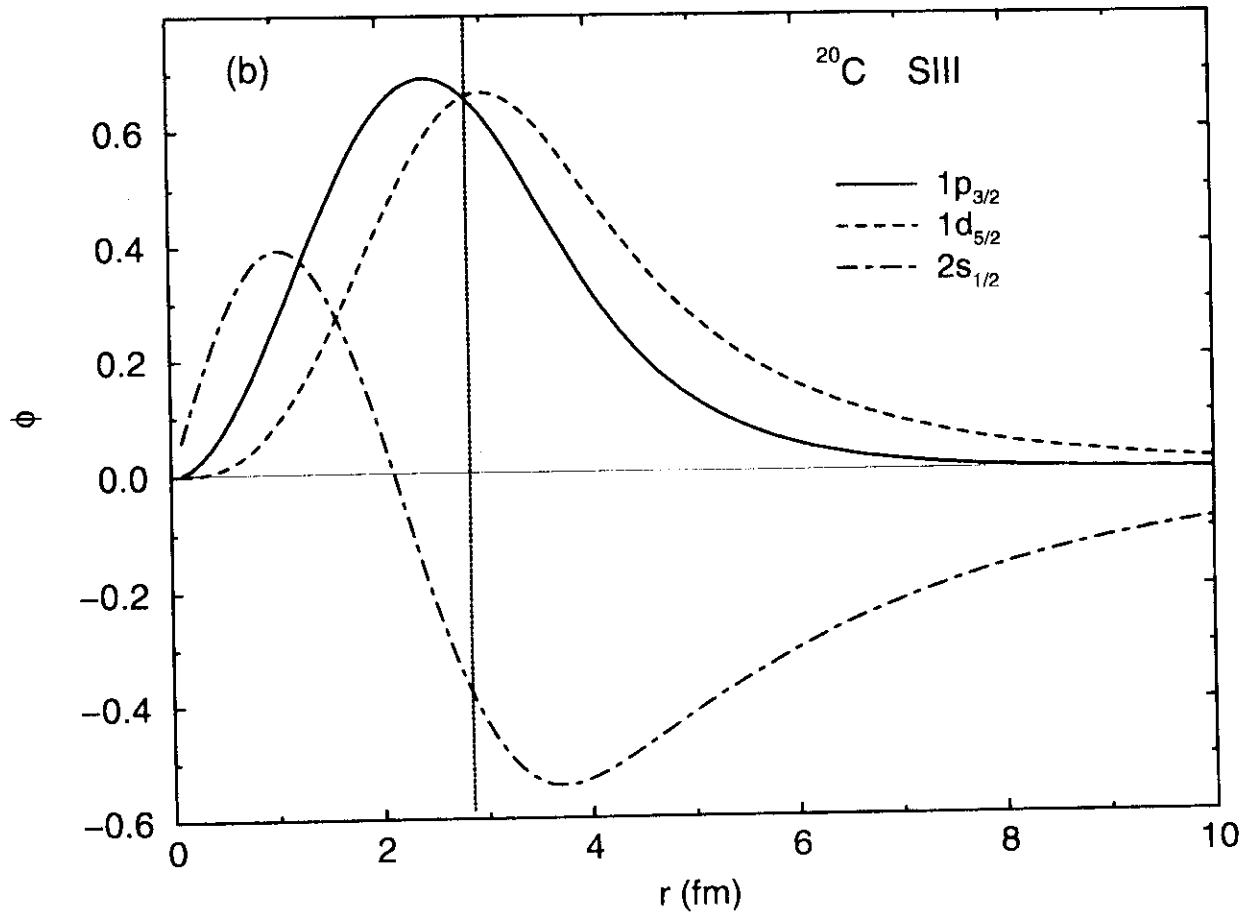
(b)
^{20}C SIII
$1p_{3/2}$
$1d_{5/2}$
$2s_{1/2}$
ϕ
0.6
0.4
0.2
0.0
−0.2
−0.4
−0.6
0
2
4
6
8
10
r (fm)

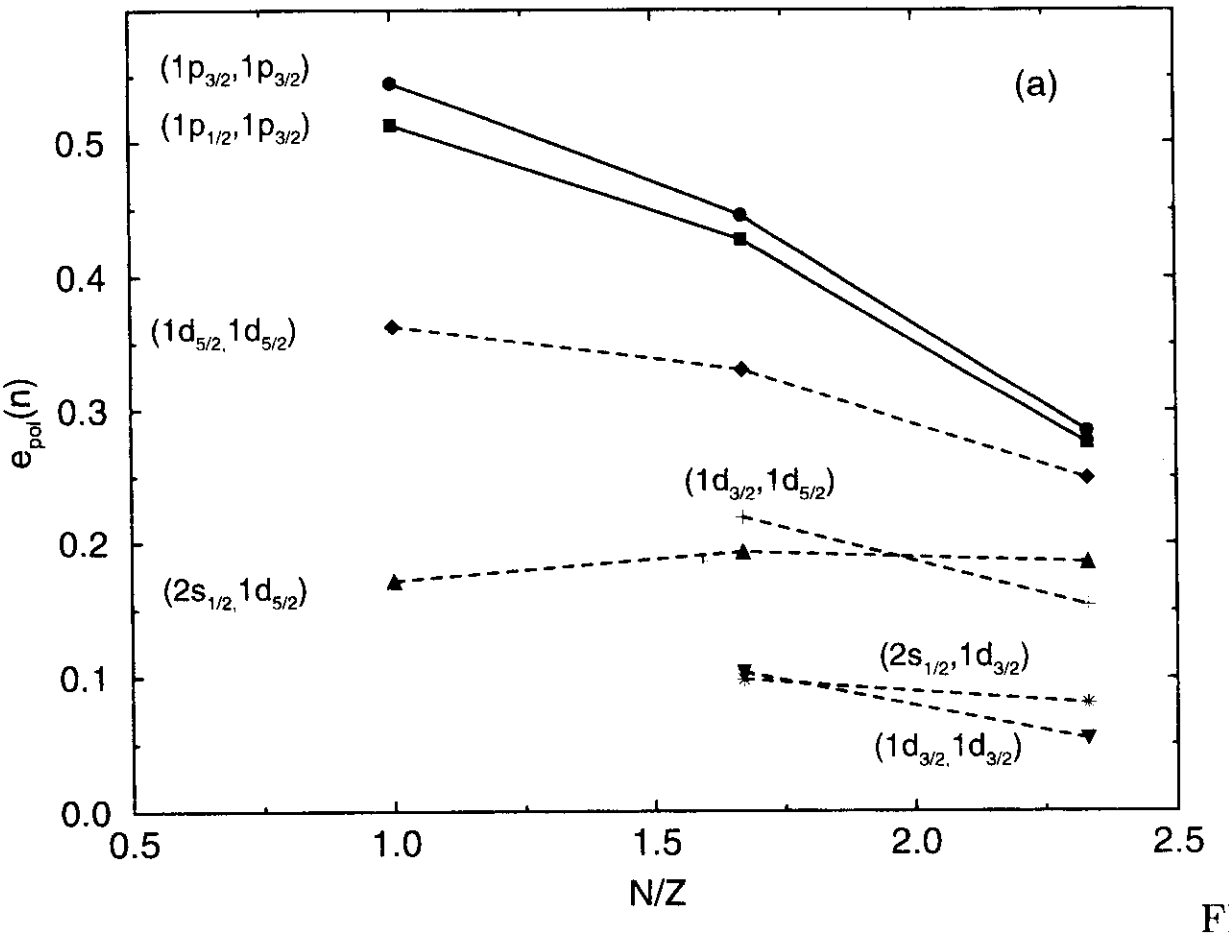
(a)
$(1p_{3/2},1p_{3/2})$
$(1p_{1/2},1p_{3/2})$
$(1d_{5/2},1d_{5/2})$
$(1d_{3/2},1d_{5/2})$
$(2s_{1/2},1d_{5/2})$
$(2s_{1/2},1d_{3/2})$
$(1d_{3/2},1d_{3/2})$
$e_{pol}(n)$
N/Z
0.0
0.1
0.2
0.3
0.4
0.5
0.5
1.0
1.5
2.0
2.5

FIG. 4.

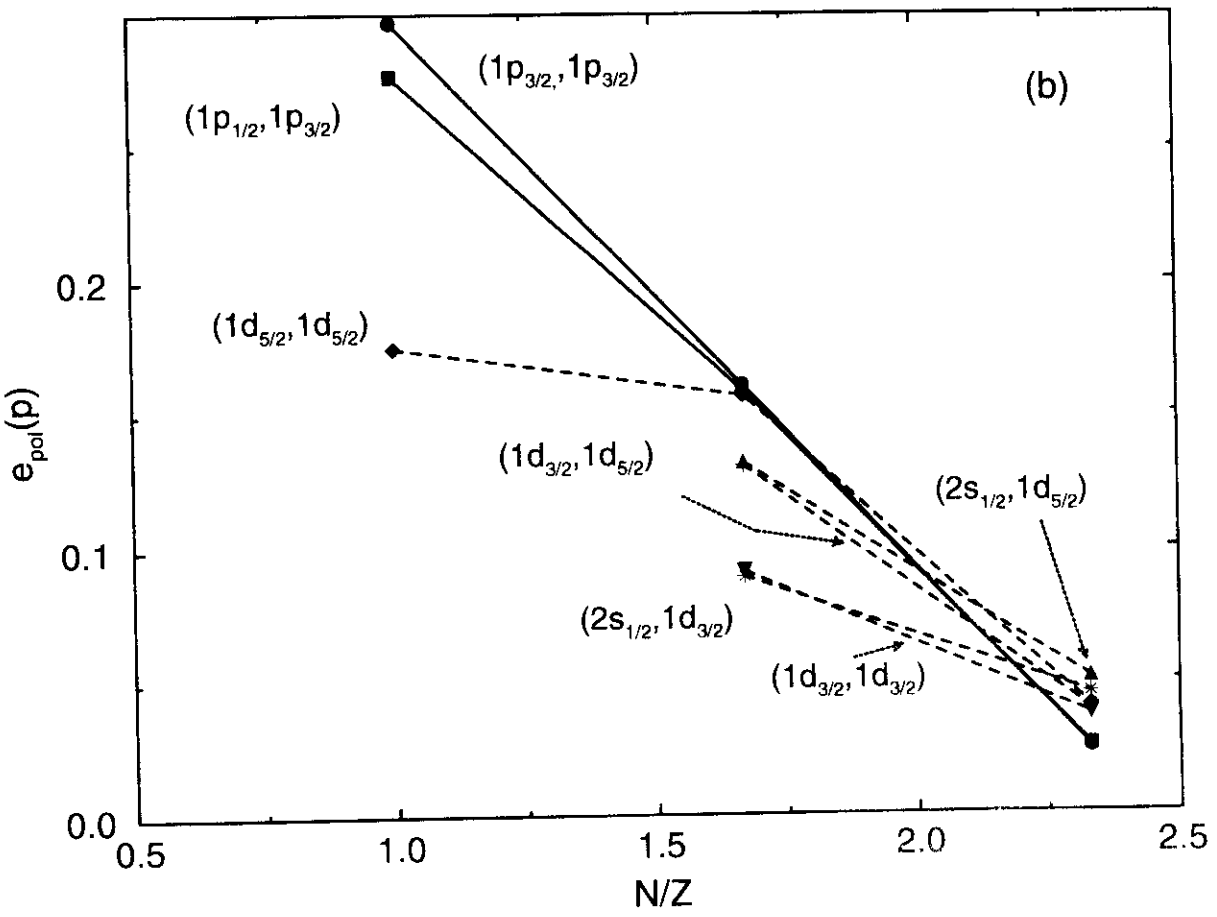
(b)
$(1p_{3/2},1p_{3/2})$
$(1p_{1/2},1p_{3/2})$
$(1d_{5/2},1d_{5/2})$
$(1d_{3/2},1d_{5/2})$
$(2s_{1/2},1d_{5/2})$
$(2s_{1/2},1d_{3/2})$
$(1d_{3/2},1d_{3/2})$
$e_{pol}(p)$
N/Z
0.0
0.1
0.2
0.5
1.0
1.5
2.0
2.5

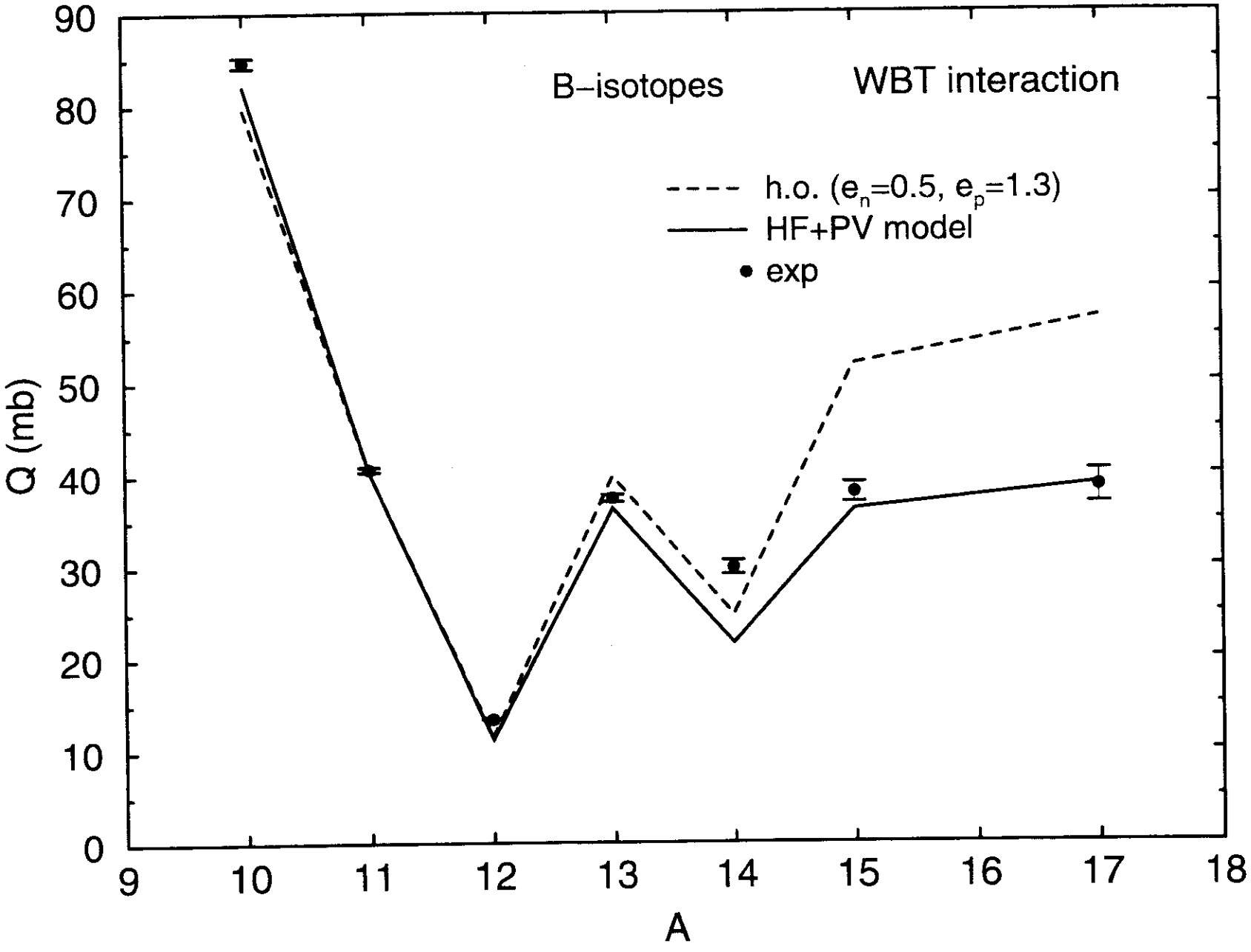
B–isotopes
WBT interaction
h.o. (e_n=0.5, e_p=1.3)
HF+PV model
exp
Q (mb)
A
0
10
20
30
40
50
60
70
80
90
9
10
11
12
13
14
15
16
17
18

FIG. 5.